IEEE Access
Multidisciplinary | Rapid Review | Open Access Journal

Received November 24, 2020, accepted December 2, 2020, date of publication December 7, 2020,
date of current version December 16, 2020.

Digital Object Identifier 10.1109/ACCESS.2020.3042787

High-Efficient and Low-Cost Biased Multilevel Modulation Technique for IM/DD-Based VLP Systems

DUCKYONG KIM[1], JONG KANG PARK[2], (Member, IEEE), AND JONG TAE KIM[1,2], (Member, IEEE)

[1]Department of Electrical and Computer Engineering, Sungkyunkwan University, Suwon 16410, South Korea
[2]School of Electronic and Electrical Engineering, Sungkyunkwan University, Suwon 16410, South Korea

Corresponding author: Jong Tae Kim (jtkim@skku.edu)

This work was supported by the Basic Science Research Program through the National Research Foundation of Korea (NRF) funded by the Ministry of Education under Grant 2018R1A2B6008072 and Grant 2020R1A6A3A13075997.

ABSTRACT In recent times, several indoor positioning systems have been actively studied for environments where satellite signals are typically degraded and disrupted. Among them, visible light positioning (VLP) has attracted wide interest owing to its advantages of high energy efficiency, broad bandwidth availability, and electromagnetic interference rejection. The performance of a VLP system highly depends on its ability to distinguish between individual signals for each channel. In this paper, we propose a new optical signal modulation technique suitable for intensity-modulation/direct-detection (IM/DD)-based VLP systems. Furthermore, we present major considerations and some constraints for evaluating the modulation technique, and show the superiority of the proposed method through comparison with various conventional schemes. The comparion simulations reported that the proposed scheme improves signal-to-noise ratio (SNR) by more than 4.6 dB, reduces channel error by 3.5 times or more, and reduces peak-to-average power ratio (PAPR) by more than 6 dB excluding time division multiple access (TDMA). The performance was also verified by the positioning experiment using an field-programmable gate array (FPGA) and simple transmission/reception hardware in a 2.0 m $\times$ 0.8 m $\times$ 1.6 m region.

INDEX TERMS Visible light positioning (VLP), intensity-modulation/direct-detection (IM/DD), multilevel Hadamard matrix, sensor signal multiplexing, code division multiple access (CDMA).

I. INTRODUCTION

In recent years, there has been much research on indoor positioning where satellite signals are typically interrupted and degraded. Indoor positioning systems (IPSs) are configured through various types of signals such as infrared, ultrasound, Bluetooth, radio frequency identification (RFID), ultra-wideband (UWB), wireless local area network (WLAN) which have problems, including short transmission distances, multipath effects, low accuracy, various signal interference, and high costs for building systems. To overcome these challenges, several studies have been conducted on visible light communication (VLC)-based positioning systems. As visible light has stronger anti-interference and does not cause electromagnetic interference, it is suitable for use in RF-sensitive areas such as hospitals and airplanes [1]–[5]. Moreover, owing to the availability of broad and high bandwidths, it is easy to multiplex between multi-channel signals [4]–[7]. By using light-emitting diodes (LEDs) as signal sources, VLC-based systems have features such as energy efficiency, low cost, and long lifetime, and significant advantages in terms of construction costs because they use the LED infrastructure already built in the environment [2]–[6], [8]. Visible light positioning (VLP) systems can be broadly classified according to receiver type and reception method. The most preferred method for low-cost and high-performance VLP systems is photodiode (PD)-based intensity-modulation/direct-detection (IM/DD). In the IM/DD system, all signals must be non-negative.

The positioning performance of the VLP system significantly depends on the receiver's ability to distinguish individual signals from those of other transmitters. The

The associate editor coordinating the review of this manuscript and approving it for publication was Zhongyi Guo.

simplest method of multiple access for distinguishing individual signals is time division multiple access (TDMA) [9]. In this method, each LED transmits a unique code sequence representing its own ID and interior coordinates in a specified time slot and remains in the ON state for the remaining time to achieve its primary function as a light source. Furthermore, direct information is transmitted individually, and no additional calculation process is required; hence, the implementation of the system is relatively simple. Another technique is code division multiple access (CDMA) [10]–[12]. In CDMA, all LEDs are assigned unique sequences that encode their information, and the receiver knows all the codes and uses them to recognize each sequence. The optical orthogonal code (OOC) method [10], which uses autocorrelation through inter-signal delay, can determine the signal of an LED asynchronously; however, it requires a long transmission length, and random delays between the LED signals can cause multiple access interference (MAI). Another method is the application of the elements of the Hadamard matrix, which is known to have orthogonality [11], [12]. The methods described above are classified as digital baseband modulation techniques, which can be implemented through unipolar signals and easily implemented by on-off keying (OOK). They have considerable advantages in terms of cost and complexity.

Meanwhile, orthogonal frequency division multiple access (OFDMA) is an asynchronous bandpass modulation scheme that is attracting attention as a modulation technique for several optical systems owing to its high-speed data transmission over distributed channels. However, it converts continuous signals into optical signals through digital-to-analog converters (DACs) and low-pass filters (LPFs), requiring analog LED drivers that have relatively high cost and do not guarantee high power efficiency [13]. Owing to the nature of the IM/DD system, all signals should have positive real values, which leads to a DC-based optical OFDM (DCO-OFDM) [14] and asymmetric clipped optical OFDM (ACO-OFDM) [15]. DCO-OFDM is a method for removing negative elements by adding a DC bias to each subcarrier. The use of a high DC bias results in a very large light energy per bit for a one-sided noise power spectrum density, making it inefficient in terms of photoelectric power. Therefore, low-bias is generally used, which causes a clipping noise that affects all the subcarrier signals. In ACO-OFDM, negative values are clipped on general OFDM signals, where only odd-order subcarriers can transmit data symbols to satisfy orthogonality. The signal stability of ACO-OFDM is relatively high because clipping does not result in loss of information due to the half-wave symmetry. However, because only odd-order subcarriers are available, the frequency efficiency is significantly reduced whereas numerous channels (2N-1 subcarriers) are required [16].

Although various types of multiple access methods applicable to the VLP system have been proposed and verified, they still have a lack of preparation to move on to the real-life application, which is the ultimate goal of the IPS. For example, in [17], [18], high accuracy three-dimensional positioning was studied by applying an artificial neural network (ANN), but due to a long operation time and a large amount of computation, these methods are difficult to apply to industry. In [19], [20], the speed of ANN was improved by efficiently reducing the data or optimizing the structure, however, the burden of collecting training data and adjusting detailed parameters, which is a problem of pre-learning-based machine learning, is still required. In [3], Cai *et al.* proposed the positioning system based on modified particle swarm optimization (PSO) algorithm that shows high localization accuracy and significantly lower algorithm complexity. On the other hand, by operating in a low frequency band of 400 Hz, this method cannot avoid interference by artificial light sources such as incandescent and fluorescent lamps. In [21], Mai *et al.* proposed a large-scale indoor positioning system using OOCs, but this method requires a long reception time of more than 1 second for a moving target, which is difficult to apply to real-time applications.

In this paper, we examine the main factors of the modulation technique for the VLP system that need to be evaluated for commercial and industrial applications. We also suggest reasonable boundaries for some options based on academic evidence, such as the maximum available frequency depending on the device's physical response time. Then we propose a new modulation technique with no order constraints and efficient power adjustment based on a multi-level Hadamard (M-H) matrix [22]–[24]. The superiority of the proposed method is verified by some simulations that compares with other methods based on the various considerations defined above. A quantitative evaluation is also provided with a practical experiment using a simple hardware configurations.

The contributions of this paper are summarized as follows:

1) We first propose a new multiple access technique suitable for an IM/DD-based VLP system using the orthogonal properties of a M-H matrix. This method can be implemented with only three levels of intensity including 0, and can be applied to both baseband and bandpass methods. The proposed method can efficiently control the peak power (amplitude) of the modulated signal while maintaining orthogonality by subtracting arbitrary bias from the M-H matrix and adding it to the post-modulation processes. Its peak-to-average power ratio (PAPR) value is 1 in the ideal case, such that this method has the largest signal dynamic range in the same active region.
2) We also define the major parameters to be considered in the modulation of the IM/DD-based VLP system. In this paper, we have an in-depth investigaion on various factors such as the number of LEDs according to the recommended indoor brightness, interference of artificial light sources, and physical characteristics of general LED and PD elements. In addition, the evaluation indicators of VLP modulation such as the degree of the channel error, the direction of multi-channel error,

and PAPR are defined. Some limitations and required specifications are also given by assuming that the VLP system is applied in the general space rather than in an ideal environment such as a laboratory. Based on these considerations, we evaluate the proposed method by comparison with other methods.

3) Finally, we experimentally validate the performance of the proposed technique in a VLP system. We implement receiver and transmitter modules controlled by field-programmable gate arrays (FPGAs), which contain digital logic designs with signal processing units. In particular, we implement the signal much simply by applying the concept of the spatial summing technique [25], [26]; three levels of signal are implemented by controlling 0, 1, and 4 LEDs simultanously. An in-depth analysis is conducted on secondary errors caused by its configuration. The positioning performance is also verified by experiments in an indoor environment.

The remainder of this paper is organized as follows. In section II, we suggest major considerations for the IM/DD-based VLP system. For some items, specific required boundaries are also suggested. In section III, we describe the basic optical model for the VLP system and propose the biased multi-level modulation technique. Here, the principle of the proposed method is explained and some calculations are made to indicate the performance. In section IV, based on the proposed considerations, we compare the results of the proposed method with those of the conventional bandpass and baseband techniques. In section V, we perform indoor positioning with the proposed method using an FPGA and simple hardware, and discuss its numerical results. Finally, we present the conclusions in section VI.

II. DESIGN CONSIDERATIONS FOR VLP SYSTEMS

A. NUMBER OF LEDs (CHANNELS)

In an indoor environment, a brightness of 400–1000 lux (= lumen/m^2) is generally required, and most of the latest LEDs have a maximum brightness of 320 lumens [27]. Assume a specific situation in which approximately 25–63 LEDs are required in a 20 m^2 space. Concentrating multiple LEDs in one spot or using high-brightness LEDs can be injurious to the human eye; hence, the LED channels should be scattered in a large space. In addition, because general VLP systems require the reception of multiple (usually three or more) optical signals, their performance near walls or various obstacles in the room will not be guaranteed with a small number of light sources. In summary, when considering various environments, it is reasonable to arrange enough LEDs to be sufficiently spread out to achieve high positioning performance.

B. ERROR DISTRIBUTION OF THE MEASURED SIGNAL STRENGTH

The effect of the received signal strength (RSS) error depends on the background environment or lighting level. Therefore, the evaluation of the RSS error is standardized in proportion to the total signal strength. The criteria for evaluating the single channel error and the overall channel error are given as:

$$\epsilon_i = \left|H_i' - H_i\right| \Big/ \sum_k^N H_k, \quad \epsilon = \sum_i^N \epsilon_i \tag{1}$$

where H_i' and H_i denote the measured channel gain and the ideal channel gain. Furthermore, because the VLP system determines the position of the receiver by gathering the RSS information of multiple channels equally, the degree of the individual errors and the tendency of the overall deduced error are important.

Figure 1 shows an example of a positioning system with three LEDs. d_i is the actual distance between the transmitter and receiver, and d_i' is the distance calculated from the measured signal strength. The calculation of d_i' is described in section III-B. If the signal strength of $\mathrm{LED_A}$ has a negative error, i.e., if the signal strength is perceived to be weaker than the original value, the positioning error of the receiver will be determined further away from $\mathrm{LED_A}$. Meanwhile, if the signal strengths of $\mathrm{LED_B}$ and $\mathrm{LED_C}$ have positive errors, the positioning error will be further away from $\mathrm{LED_A}$ (Fig. 1b). By contrast, if the signal strengths of $\mathrm{LED_B}$ and $\mathrm{LED_C}$ have negative errors similar to $\mathrm{LED_A}$, the positioning error will be further away from all the LEDs such that the receiver has a negligible positioning error (Fig. 1c). Similarly, when all the LEDs have positive errors, the positioning error will be small. Thus, although the magnitude of the absolute error for each channel is the same, the direction of the errors is very important in determining the positioning error. The evaluation criteria for the single-channel directional error and overall channel directional error applied in this study are given as:

$$E_i = \left(H_i' - H_i\right) \Big/ \sum_k^N \left|H_k' - H_k\right|, \quad E = \left|\sum_i^N E_i\right|. \tag{2}$$

The performance evaluation related to signal strength errors is described in more detail in section IV.

C. RESPONSE TIME

One of the important considerations for the VLP system is the real-time recognition of a moving target. When the position of the receiver changes, each channel information also changes in real-time; hence, the ability of the system to analyze and process signals as quickly as possible is important. We suggest that the positioning should be performed at least 10 times per second.

In the VLP system, various information, including individual ID, location, and signal characteristics of each LED must be transmitted. In this paper, we consider the transmission of 128 bits for the LED information, 8 bits each for the beginning and end flags, and 16 bits for the cyclic redundancy check (CRC) within one frame [28]. Thus, the required minimum data rate is (128+8+8+16) bits / 0.1 s = 1.6 Kbps.

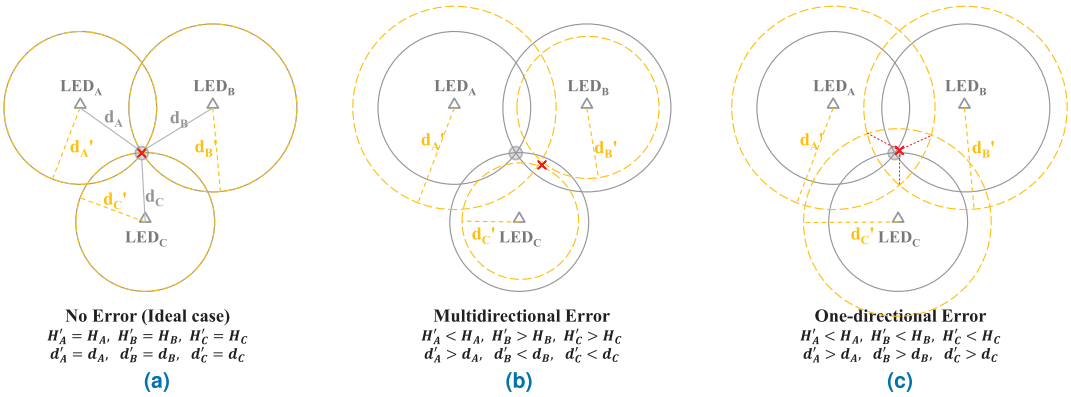

FIGURE 1. Example of a positioning system using 3 LEDs.

D. MODULATION FREQUENCY (BANDWIDTH)

Human eyes can detect up to 75 Hz in stable conditions and up to several 100 Hz in rapid movement. If the system is operated under this condition, it can cause an annoying flickering effect. Hence, it is necessary to operate the system at a frequency of 200 Hz or higher [29].

Another important factor to be considered is interference by artificial light sources, especially in the indoor positioning environment. Artificial light sources, including incandescent and fluorescent lamps, generate periodic and deterministic interference signals [30]. In the case of incandescent lamps, the interference spectrum can extend up to 2 kHz, whereas for fluorescent lamps driven by conventional and electronic ballasts, the interference spectra can extend up to 20 kHz and 1 MHz, respectively. We propose a frequency of 25 kHz or higher, considering the influence of existing ballasts on fluorescent lamps.

Moreover, the physical response of the LED and PD must be considered. The period of the signal must be greater than the transition time according to the ON and OFF operations of the LED ($0.5/f > \tau_{\text{on}} + \tau_{\text{off}} = \tau_{\text{LED}}$). This value is determined by the phosphor plating of the LED and is typically 20 ns [27]. In other words, the maximum usable frequency is theoretically $f_{\text{MAX}} = 0.5/(20 \times 10^{-9}) =$ 25 MHz. We suggest a frequency range within a few MHz to ensure stable signal transmission. Because the response of PD is much faster than that of LED, it may not be considered [31], [32].

E. DESIGN FOR LOW-COST, HIGH-EFFICIENT SYSTEM

For a low-cost system design, the complexity and cost of the LED driver circuit must be low. The simplest way is to drive the LEDs as binary (ON/OFF). It is also recommended to minimize the number of crystal oscillators in the clock inaccuracy and cost between the channels.

Another key factors for the low-cost design of multi-channel transmission/reception systems is the PAPR [33], which is the ratio of the maximum power of a signal to its average power. When the PAPR is high, the dynamic range increases and the signal peak can be saturated, thereby entering the nonlinear region of the power amplifier and causing signal distortion. To prevent this, the active region of the amplifying circuit must be sufficiently large, which increases the hardware design complexity and power consumption. PAPR is calculated using:

$$\text{PAPR}\,(x\,[n]) = \frac{\max(|x\,[n]|^2)}{\text{E}[|x\,[n]|^2]}. \tag{3}$$

III. SYSTEM DESIGN

A. OPTICAL MODEL

Generally, LED signals are treated as Lambertian sources owing to their large beam divergence in indoor environments. Thus, in a line-of-sight (LOS) condition, the wireless channel DC gain H follows the Lambertian radiation as follows [2], [7], [14]:

$$H = \frac{(m+1)A}{2\pi d^2}\cos^m\phi\cos^n\psi T_s(\psi)g(\psi)rect\left(\frac{\psi}{\text{FOV}}\right) \tag{4}$$

where A is the physical area of the detector, d is the distance between the LED and the PD, and ϕ and ψ are the radiation and incidence angles with respect to the transmitter and receiver, respectively. Order m is related to $\phi_{1/2}$, which is the transmitter half-angle, defined by $m = \frac{-\ln 2}{\ln(\cos(\phi_{1/2}))}$. Similarly, order n is related to the receiver half-angle, $\psi_{1/2}$, defined by $n = \frac{-\ln 2}{\ln(\cos(\psi_{1/2}))}$. $T_s(\psi)$ is the optical gain of the filter, and $g(\psi)$ is the concentrator gain. Finally, rect(x) is a rectangular function defined by rect(x) $= 1$ for $|x| \leq 1$, otherwise rect(x) $= 0$. If the field-of-view (FOV) of the receiver is sufficiently large such that $0 \leq \psi \leq$ FOV is satisfied, then rect(ψ/FOV) is always equal to unity. For simplicity, several studies have ignored the effects of the filter and concentrator and have replaced them with constant values [3], [9]. In this work, we also consider the effect of the filter and the concentrator as constant 1.

In this paper, it is assumed that the receiver is placed horizontally with respect to the ground; hence, $\cos\phi = \cos\psi = h/d$ is established, where h is the height of the LED.

Accordingly, (4) is simplified as follows:

$$H = \frac{(m+1)A}{2\pi d^2} T_s(\psi) g(\psi) \cdot \left(\frac{h}{d}\right)^{m+n} = \frac{(m+1)AT_s(\psi)g(\psi)h^{m+n}}{2\pi} \cdot \left(\frac{1}{d}\right)^{m+n+2}. \quad (5)$$

Most visible light systems operate in environments with various types of infrared and visible background light. Although the received background lighting can be minimized by optical filtering, it typically results in shot noise, which is a limited noise source for well-designed receivers [2]. The shot noise can be modeled as an independent white Gaussian noise owing to its high intensity. If the ambient light is sufficiently low, the dominant noise source can be thermal noise, which is also independent and Gaussian. Therefore, we modeled the general system noise as an independent Gaussian noise with the total variance of the shot and thermal noises as follows [2]:

$$\sigma_{total}^2 = \sigma_{shot}^2 + \sigma_{thermal}^2. \quad (6)$$

In the simulation described in the section below, we treat all system noise sources as white Gaussian noise.

B. POSITIONING ALGORITHM

In this study, we performed positioning using the trilateration method. First, three signals with the highest signal strength are selected among each received channel signal. Let the positions of the three transmitters and one receiver be denoted as (x_1, y_1, h), (x_2, y_2, h), (x_3, y_3, h), $(x, y, 0)$ and the distance between the transmitter and receiver be d_1, d_2, and d_3; the distance for each channel can be calculated as:

$$\begin{cases} d_1^2 = (x_1 - x)^2 + (y_1 - y)^2 + h^2 \\ d_2^2 = (x_2 - x)^2 + (y_2 - y)^2 + h^2 \\ d_3^2 = (x_3 - x)^2 + (y_3 - y)^2 + h^2. \end{cases} \quad (7)$$

Additionally, let the three signal strengths be H_1, H_2, and H_3. The distance d_i from each transmitter can be calculated using

$$d_i = \left(\frac{(m+1)\,AT_s(\psi)\,g(\psi)\,h^{m+n}}{2\pi H_i}\right)^{\frac{1}{m+n+2}} \quad (8)$$

Equation (7) can be expressed in matrix form as follows:

$$\boldsymbol{BX} = \boldsymbol{C} \quad (9)$$

where

$$\boldsymbol{B} = \begin{bmatrix} x_2 - x_1 & y_2 - y_1 \\ x_3 - x_1 & y_3 - y_1 \end{bmatrix}, \quad \boldsymbol{X} = \begin{bmatrix} x \\ y \end{bmatrix}, \quad \boldsymbol{C} = \begin{bmatrix} \left(d_1^2 - d_2^2 + x_2^2 + y_2^2 - x_1^2 - y_1^2\right)/2 \\ \left(d_1^2 - d_3^2 + x_3^2 + y_3^2 - x_1^2 - y_1^2\right)/2 \end{bmatrix}. \quad (10)$$

Here, the coordinates of the receiver can be obtained by using the linear least square method as follows:

$$\boldsymbol{X} = \left(\boldsymbol{B}^\top \boldsymbol{B}\right)^{-1} \boldsymbol{B}^\top \boldsymbol{C}. \quad (11)$$

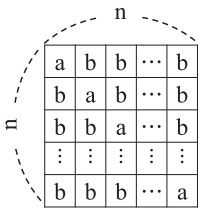

FIGURE 2. Conventional multi-level Hadamard matrix.

C. MODULATION TECHNIQUE WITH MODIFIED MULTI-LEVEL HADAMARD CODE

In this paper, we propose a biased M-H (BMH) code that can easily adjust the average power of the entire system while maintaining the orthogonality of the conventional M-H matrix to be applied to a new visible light modulation system. A conventional M-H matrix comprises a diagonal component a and the remaining components b. If the order of the M-H matrix is defined as n and the sum of columns or rows as m, $a = m(2/n - 1)$ and $b = 2m/n$. The sum of each row or column of the M-H matrix can be derived as $a + (n-1)\,b = m$, and is perfectly orthogonal to each row by $2ab + (n-1)\,b^2 = 0$. Figure 2 illustrates the kernel structure of the M-H matrix with any order of n.

Because the sum of all the rows and columns is the same, M-H has an advantage in that it is easy to control the average signal sum. As a matrix can be expressed for all arbitrary n, there is no restriction on any order, which is a significant advantage of this method compared to the conventional CDMA method. For example, in the case of a commonly used Walsh–Hadamard (W–H) method, the order of the matrix is restricted to 2^k, and in the regular Hadamard matrix, it is restricted to $4u^2$ [34]. Particularly, as the number of channels increases, the gap in the usable order considerably increases.

In this paper, we propose a BMH code that efficiently manages the average power consumption of the system while maintaining orthogonality. Let the sum of the columns and rows of the M-H be m. To reduce the total power of the transmitted signals, the sum of the columns and rows is $m - n \cdot b_m$ is calculated by subtracting the value of b_m from all the matrix components. The value of b_m can be arbitrarily set, and if it is set to m/n, the sum of the columns and rows becomes zero, resulting in the most power-efficient case. In other words, within the same active region of the receiver amplifier circuit, the dynamic range of the transmission signal becomes very large. The substracted portion can be restored to the original orthogonal M-H signal by adding the sum of all the original signals to the received signal. This process can be expressed using the following equations:

$$\boldsymbol{r} = \boldsymbol{s} \times \boldsymbol{H}_{\mathbf{BMH}} + \boldsymbol{z} = \boldsymbol{s} \times (\boldsymbol{H}_{\mathbf{MH}} - b_m \boldsymbol{J}) + \boldsymbol{z} = \boldsymbol{s} \times \boldsymbol{H}_{\mathbf{MH}} - b_m \cdot sum(\boldsymbol{s}) + \boldsymbol{z} \quad (12)$$

$$\boldsymbol{r}^* = \boldsymbol{r} + b_m \cdot sum(\boldsymbol{s}) = \boldsymbol{s} \times \boldsymbol{H}_{\mathbf{MH}} + \boldsymbol{z} \quad (13)$$

$$\boldsymbol{s}^* = \boldsymbol{r}^* \times \boldsymbol{H}_{\mathbf{MH}}{}^\top = (\boldsymbol{s} \times \boldsymbol{H}_{\mathbf{MH}} + \boldsymbol{z}) \times \boldsymbol{H}_{\mathbf{MH}}{}^\top = \boldsymbol{s} \times m^2 \boldsymbol{I} + \boldsymbol{z}' \quad (14)$$

where $\boldsymbol{r}$ is the received modulation signal, $\boldsymbol{s}$ is the RSS of each transmitted channel, $\boldsymbol{H_{BMH}}$ and $\boldsymbol{H_{MH}}$ are the modified M-H and the original matrices, respectively, b_m is the bias applied to BMH, $\boldsymbol{J}$ is a $n \times n$ matrix with all elements equal to 1, z and z' are a $1 \times n$ white Gaussian noise matrix, $\boldsymbol{r^*}$ is a post-processed reception signal obtained by reconstructing the modulated BMH signal into an M-H signal, and $\boldsymbol{s^*}$ is the obtained transmission signal demodulated through the orthogonality of M-H with the restored reception signal.

The effect of biasing is shown below. Let the RSS transmitted by each TX be s_i and its average be E[$\boldsymbol{s}$]. The received signal in each time slot r_i is given by:

$$\begin{aligned} r_i &= \sum_{k}^{n} s_{k(\neq i)} \cdot b' + s_i \cdot a' \\ &= \sum_{k}^{n} s_{k(\neq i)} \cdot \left(\frac{2m}{n} - b_m\right) + s_i \cdot \left(\frac{2m}{n} - m - b_m\right) \\ &= \sum_{k}^{n} s_k \cdot \left(\frac{2m}{n} - b_m\right) - s_i \cdot m. \end{aligned} \tag{15}$$

Here, the received signals of the conventional M-H with $b_m = 0$ and the modified M-H with $b_m = m/n$ are given as (16) and (17), respectively,

$$\begin{aligned} r_{i,\mathrm{MH}} &= \sum_{k}^{n} s_k \cdot \frac{2m}{n} - s_i \cdot m \\ &= E[\boldsymbol{s}] \cdot 2m - s_i \cdot m = m(2E[\boldsymbol{s}] - s_i) \end{aligned} \tag{16}$$

$$\begin{aligned} r_{i,\mathrm{BMH}} &= \sum_{k}^{n} s_k \cdot \frac{m}{n} - s_i \cdot m \\ &= E[\boldsymbol{s}] \cdot m - s_i \cdot m = m(E[\boldsymbol{s}] - s_i) \end{aligned} \tag{17}$$

and the average power of the received signal is given as:

$$\begin{aligned} P_{\mathrm{MH}} &= E\left[\boldsymbol{r_{MH}}^2\right] = m^2 E\left[(2E[\boldsymbol{s}] - \boldsymbol{s})^2\right] \\ &= m^2 E\left[4E[\boldsymbol{s}]^2 - 4E[\boldsymbol{s}]\boldsymbol{s} + \boldsymbol{s}^2\right] \\ &= m^2 E\left[\boldsymbol{s}^2\right] \end{aligned} \tag{18}$$

$$\begin{aligned} P_{\mathrm{BMH}} &= E\left[\boldsymbol{r_{BMH}}^2\right] = m^2 E\left[(E[\boldsymbol{s}] - \boldsymbol{s})^2\right] \\ &= m^2 E\left[E[\boldsymbol{s}]^2 - 2E[\boldsymbol{s}]\boldsymbol{s} + \boldsymbol{s}^2\right] \\ &= m^2 E\left[E[\boldsymbol{s}]^2 - \boldsymbol{s}^2\right] = m^2\sigma_s^2 \end{aligned} \tag{19}$$

where σ_s denotes standard deviation of the transmitted signals. (18) and (19) show that the average power consumption of BMH is considerably lower than that of the conventional M-H. In addition, because the BMH power consumption is proportional to σ_s^2, it approaches zero as the magnitude of each transmission signal is similar to each other.

Furthermore, the PAPR of the methods is derived. Assuming $min[\boldsymbol{s}] = E[\boldsymbol{s}] - \sigma_s$, the $max[\boldsymbol{r_{MH}}]$ and $max[\boldsymbol{r_{BMH}}]$ values are calculated using (16) and (17), which gives as:

$$\mathrm{PAPR_{MH}} = \frac{max\left[\boldsymbol{r_{MH}}^2\right]}{E\left[\boldsymbol{r_{MH}}^2\right]} = \frac{(m(E[\boldsymbol{s}] + \sigma_s))^2}{m^2 E\left[\boldsymbol{s}^2\right]}$$

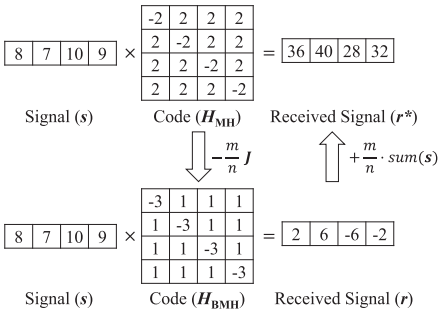

FIGURE 3. Example of modulation using M-H and BMH methods.

$$= \frac{(E[\boldsymbol{s}] + \sigma_s)^2}{E\left[\boldsymbol{s}^2\right]} = 1 + \frac{2E[\boldsymbol{s}]\sigma_s}{E\left[\boldsymbol{s}^2\right]} \tag{20}$$

$$\mathrm{PAPR_{BMH}} = \frac{max\left[\boldsymbol{r_{BMH}}^2\right]}{E\left[\boldsymbol{r_{BMH}}^2\right]} = \frac{(m\sigma_s)^2}{m^2\sigma_s^2} = 1 \tag{21}$$

It shows that the PAPR of the proposed method is 1, which is the most ideal value. It means that the proposed method operates with the minimum dynamic range and can utilizes the power amplifier, which is the most power-consuming and costly component, very efficiently.

Figure 3 shows an example of driving the conventional M-H with $n = 4$ and $m = 4$ and the BMH with $b_m = m/n$. It can be seen that the overall signal efficiency of the BMH method is higher than that of the M-H method.

We designate elements of BMH as $a' = a - b_m$ and $b' = b - b_m$, respectively. In this study, the Manchester coding scheme was applied to transmit a negative signal related to element a' in an IM/DD system that transmits only non-negative values. To recover the M-H received signal $\boldsymbol{r^*}$, the $sum(\boldsymbol{s})$ value must also be transmitted; hence, after n time slots, a signal of length $n \times 0.1$ is added to transmit b' signals in all the TXs. The specific structure of the hardware is described in section V.

IV. COMPARISON WITH OTHER METHODS

In this section, we compare the performance of the proposed method with other conventional multiple access techniques based on the considerations described in section II. As mentioned in section II, the signal error, error direction, sensing speed (response time), and PAPR are evaluated. In this section, we compare the signal-to-noise ratio (SNR) value of all the methods proportional to the same sensing time. The signal frequency was designed to be 500 kHz to satisfy the proposed conditions mentioned in subsection II-D. The OFDM method, which requires various subcarrier frequencies, was designed to use n subcarriers in which the greatest value of the fundamental frequency was 500 kHz.

A. COMPARISON WITH CDM, TDM (DIGITAL BASEBAND TRANSMISSION)

For the comparison, three-level OOK, including 0 for BMH, and two-level OOK for CDM and TDM were implemented, and all the methods were driven at 500 kHz frequency. In the

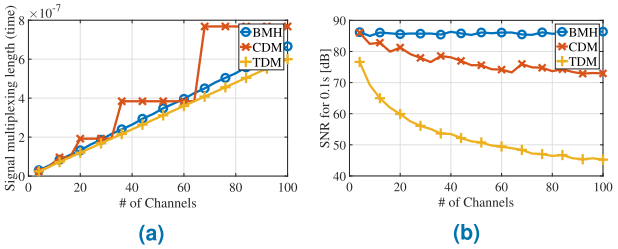

FIGURE 4. Sensing time and unit time SNR according to the number of channels of each baseband method.

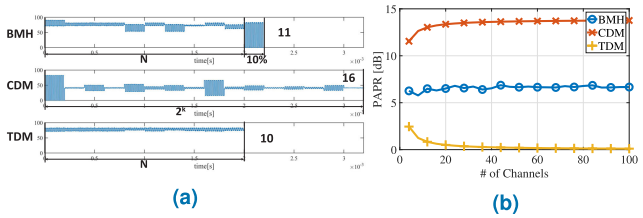

FIGURE 5. Waveform example and PAPR value of each baseband method.

CDM method, the W-H matrix, which is the most commonly used matrix, was applied. Meanwhile, all the methods were driven to repeatedly transmit signals 10 times for each slot for accurate recognition.

Figure 4 shows the plot of the sensing time of the methods and the unit-time SNR based on the number of channels. Because the CDM method operates based on the W-H matrix with a degree of 2^k, the total sensing time increased discretely according to the order constraint. Meanwhile, the TDM method used n slots, while BMH required an additional 10 % of the sensing time to transmit the sum value. The unit-time single-channel SNR was calculated considering that the system is operated every 0.1 s. As shown in the figure, the SNR of the proposed method is the best among the three methods.

Figure 5 shows the waveform of the received signal when $n = 100$ and the PAPR of each method based on the number of channels. In the CDM method, the signal period was long according to the order condition of the W-H matrix. Moreover, because the element value of the first row is 1 for all the signals, the size of the first slot and the PAPR value were relatively large. As TDM uses only n slots, the signal length was short. Furthermore, by keeping all the $n - 1$ LEDs that are not related to each slot as "On," the average power was significantly high, whereas the PAPR became relatively low. However, the BMH had a slightly longer waveform than TDM because of its short extra length, and a relatively high PAPR that is significantly higher than that of CDM.

In Fig. 6, the single-channel SNR, channel error ϵ, error direction E, and positioning error based on the system SNR are compared. As shown in the figure, the TDM method has had poor results in all aspects, and E is low in the CDM method. While the CDM method had a relatively good SNR

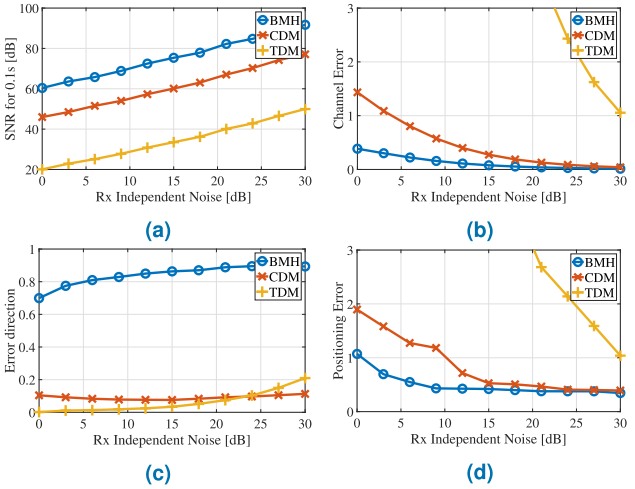

FIGURE 6. SNR, channel error, error direction, and positioning error of each baseband method.

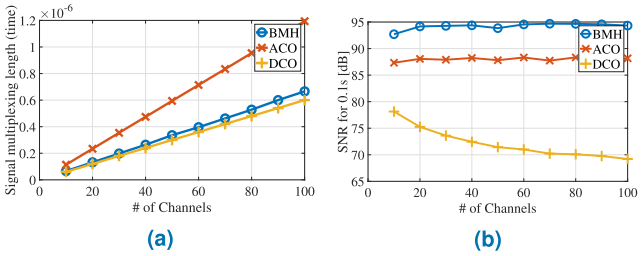

FIGURE 7. Sensing time and unit time SNR according to the number of channels of each bandpass method.

and positioning error, the proposed method was superior in terms of SNR, ϵ, and positioning error.

Overall, when n is sufficiently large ($n = 100$), the proposed method has a PAPR of about 6 dB higher than that of TDM, but an SNR of 40 dB better, and a PAPR of about 8 dB lower and an SNR of about 15 dB better than that of CDM. Also, the channel error is 3.5 to 90 times better than the two methods.

B. COMPARISON WITH OFDM (BANDPASS TRANSMISSION)

In this comparison, BMH was driven at a 500 kHz frequency and was implemented to clip negative signals such as ACO-OFDM. In the OFDM method, the subcarrier frequency was set such that the greatest subcarrier frequency was 500 kHz. For example, in the case of $n = 4$, DCO-OFDM uses a fundamental frequency of 125 kHz and a multiple of its subcarrier frequency, whereas ACO-OFDM uses a fundamental frequency of 55.6 kHz and an odd number of subcarriers. BMH repeatedly transmits the signal three times per slot and proportionally repeats the OFDM signal.

Figure 7 shows the plots of the sensing time and the SNR based on the number of channels. As mentioned in section I, because ACO-OFDM requires $2n - 1$ sub-frequencies, it has to deal with a relatively lower frequency, which results

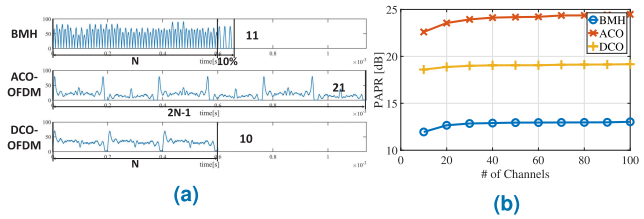

FIGURE 8. Waveform example and PAPR value of each bandpass method.

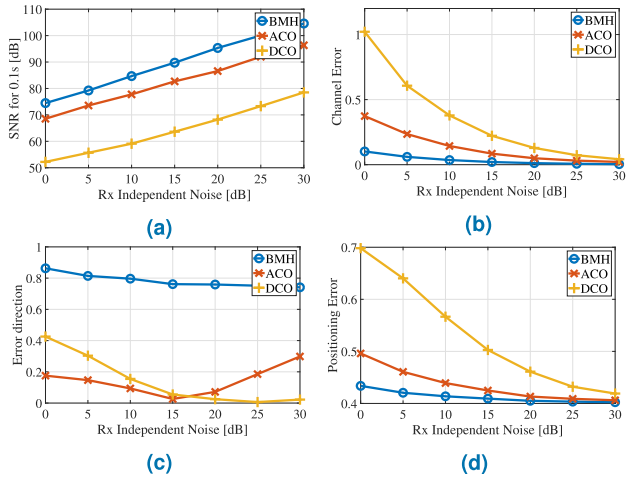

FIGURE 9. SNR, channel error, error direction, and positioning error of each bandpass method.

in a longer overall sensing time. Meanwhile, the SNR of DCO-OFDM continued to decrease, whereas the SNR of BMH was superior to that of both methods.

Figure 8 shows an example of the waveforms of the received signals of each method when $n = 10$. ACO-OFDM had a longer cycle and a higher PAPR for one whole transmission owing to the need for more fundamental frequencies, whereas DCO-OFDM had a relatively shorter cycle and a lower PAPR. Moreover, the length of BMH was partially increased compared to that of DCO-OFDM owing to the short additional length, and its PAPR was superior to that of both signals.

Figure 9 shows the comparison of the SNR, ϵ, E, and positioning errors of the three methods. In the case of DCO-OFDM, the effect of clipping noise on all the channels deteriorated the SNR and ϵ, whereas the proposed method is superior to the OFDM method for all the comparisons.

Overall, when n is sufficiently large ($n = 100$), the proposed method has a PAPR of about 11.5 dB lower and an SNR of 4.6 dB better than that of ACO-OFDM, and a PAPR of about 6 dB lower and an SNR of about 25 dB better than that of DCO-OFDM. Also, the channel error is 4.3 to 10.6 times better than the two methods.

V. EXPERIMENT RESULTS AND DISCUSSION

In this study, positioning was conducted using the BMH modulation technique, and the performance was quantitatively analyzed. The order n of the applied BMH is 5. Assuming that the sum of columns m is 5 and the bias b_m is m/n, elements of the BMH are $a' = m(2/n - 1) - m/n = -(n-1)m/n = -4$ and $b' = 2m/n - m/n = m/n = 1$. To implement this scheme, three levels of a', b', and zero should be generated, and we demonstrate that they can be implemented using a simple and inexpensive configuration with sufficiently excellent results. Additionally, the applicability of the proposed method is evaluated through a valid analysis of the experimental results.

A. EXPERIMENT SETUP

In this work, we implemented LED and PD modules that could be individually controlled by an FPGA. The experiment was conducted within a 2.0 m × 0.8 m × 1.6 m space in the laboratory. In the transmission part, each LED module was composed of four white LEDs (DG-82A83C-001), and the current was supplied through the main board with the FPGA so that one or four LEDs could be turned "On" and "Off" simultaneously. The receiver is composed of a silicon PIN photodiode (SD 100-14-21-021), and it delivers the received information through a 12-bit A/D converter operating at 12 MHz.

Figure 10 shows the overall signal processing procedure. To implement both a' and b' signals, we adopted the structure of driving one or four LEDs simultaneously: only one LED was driven for the b' signal of level 1 and four LEDs were driven simultaneously for the a' signal of level 4. Each signal of the transmitter was mixed with a 50 kHz oscillator and converted into a Manchester-coded form. The converted electrical signal was then emitted from the LEDs through the current driver. Afterward, the PD received the sum of the optical signals degraded by s_i from each LED. The signal received from the PD was then sent to the FPGA through a 12-bit ADC, and in-phase/quadrature (IQ) demodulation was performed on the received signal. Meanwhile, the received M-H value that should have been received was restored using the $sum(\boldsymbol{s})$ value received from the additional slot. The signal component RSS for each LED was extracted by multiplying each row of the M-H by the restored received value $\boldsymbol{r}^*$. Subsequently, the channel gain for each LED was obtained and the position of the receiver was estimated.

Figure 11 shows the transmitter and receiver used in this experiment. Figure 11a shows the configuration of the transmitter, including five LED boards for driving the LEDs and a main board for controlling each board. On the main board, the current supplied to each LED board was properly controlled through a switching circuit with an NPN transistor that uses the FPGA signal as a base (B). Meanwhile, all the current sources were supplied through a power supply. The LED board was composed of four LED elements and three terminals: one positive terminal providing current to all the LEDs and a negative terminal connected to each single LED and a bundle of three LEDs. When the terminals of the board were directed downward, the lower right element had a single operation and the remaining three elements operated

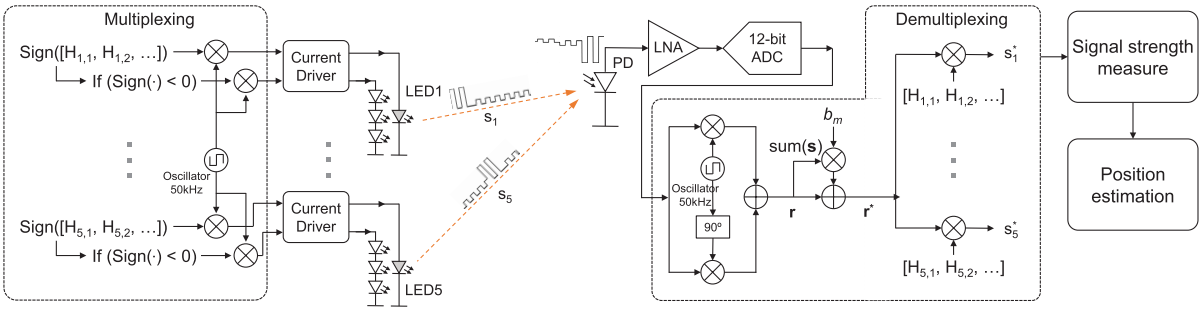

FIGURE 10. Overall signal processing flow diagram.

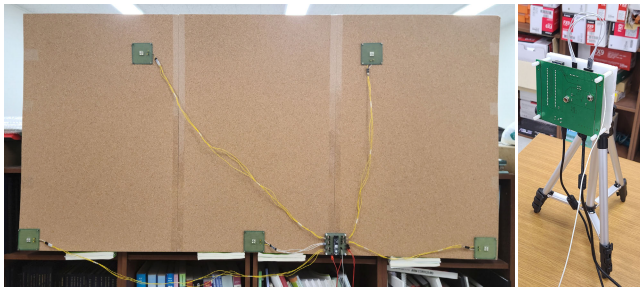

(a) Transmitter (5 LED arrays, FPGA)

(b) Receiver (PD, FPGA)

FIGURE 11. Hardware configuration for the experiment.

simultaneously. Furthermore, the five LED boards were arranged in an approximately 0.87 m long equilateral triangle pattern on a flat plate. Figure 11b shows the configuration of the receiver. The signal passing through the PD and low-noise amplifier (LNA) was delivered to the FPGA module through a 12-bit ADC. The receiver PCB was attached to a holder so that it could be easily fixed to the designated position. For accurate and precise signal transmission, the receiver and transmitter were wired to synchronize with each other.

B. EXPERIMENT RESULT

In this work, we used the trilateration method, as mentioned in subsection III-B. The five LED coordinates were (−0.87 m, 0 m), (−0.44 m, 0.72 m), (0 m, 0 m), (0.44 m, 0.72 m), and (0.87 m, 0 m). The third LED was set as the origin (0 m, 0 m, 0 m), and the height of the receiver (Z-axis) was fixed at 1.6 m. A total of 27 measurement positions were set at intervals of 0.2 m horizontally and vertically and approximately 0.14 m diagonally. The parameters of the positioning are summarized in Table 1.

The overall positioning results are shown in Fig. 12. The five LED modules are marked with a hollow purple square, and the position of a single driven LED in each module is marked with a solid purple square. For each test case, the measured location is marked with black X, the predicted position is marked with red O, and each case is labeled with a number. Here, we need to carefully observe the magnitude

TABLE 1. Parameters of the positioning system.

Parameter	Value
Space Size (L × W × H) / m	2.0 × 0.8 × 1.6
LED Position (x, y) / m	LED1 (-0.87, 0) LED2 (-0.44, 0.72) LED3 (0, 0) LED4 (0.44, 0.72) LED5 (0.87, 0)
The FOV of the LEDs / deg	120
The FOV of the PD / deg	82
The optical filter gain ($T_s(\psi)$)	1.0
The optical concentrator gain ($g(\psi)$)	1.0
Height of the receiver (h) / m	1.6
Plane position of the receiver (x, y) / m	(-0.6, 0.0) to (0.6, 0.0), (-0.5, 0.1) to (0.5, 0.1), (-0.4, 0.2) to (0.4, 0.2), (-0.3, 0.3) to (0.3, 0.3), (-0.4, 0.4) to (0.4, 0.4), 0.2 interval for x-axis

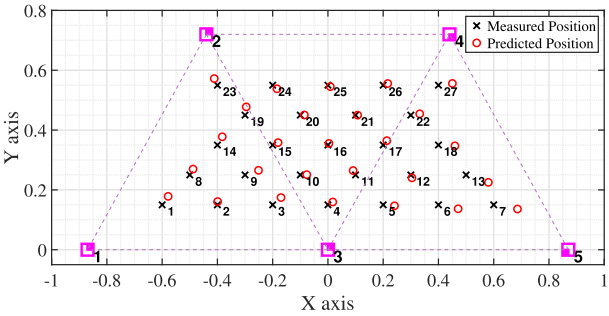

FIGURE 12. Position estimation results.

and direction of the error, i.e., the direction of the predicted position based on the measured position. In this regard, an in-depth analysis will be covered in subsection V-C. The average error of the experimental results was obtained as 3.18 cm.

The cumulative distribution function (CDF) of the errors is depicted in Fig. 13. As Fig. 13 shows, the positioning algorithm performs well in this experiment, and most of the errors are under 8 cm. To better present the error, the distribution of the errors is shown in Fig. 14. It can be seen that most of the positioning errors are within 5 cm, which proves that the positioning algorithm performed considerably well.

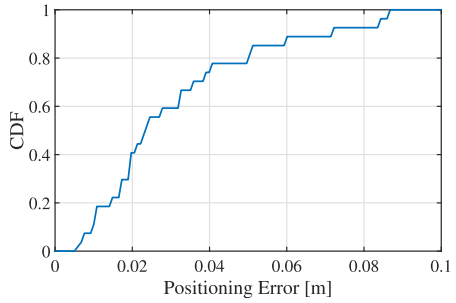

FIGURE 13. Cumulative distribution function (CDF) curves of positioning error.

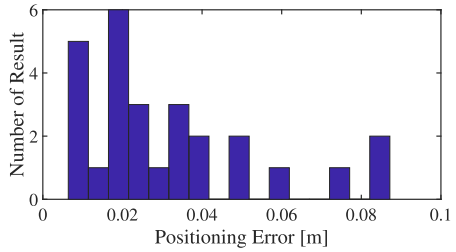

FIGURE 14. Histogram of the positioning error.

The main causes of the positioning error are summarized as follows. First, shot and thermal noise effects were observed at the PD. Second, measurement errors occurred; for example, when setting the measurement position of the receiver, the ideal and actual values may have differed slightly. In addition, other noise components occurred from the internal noise of the transmitting/receiving board, including ADC noise and noise from the power and ground. Furthermore, the LED light may have been reflected by the walls, ceiling, desk, and other obstacles within the room, thereby causing multipath effects.

C. DISCUSSION OF ERROR TENDENCY

As mentioned in subsection V-A, we implemented multilevel driving by operating zero, one, and four LEDs simultaneously. In this process, the degree of the pattern that the LED bundle affects slightly varies depending on the arrangement of the four LEDs and the viewing direction. These actions are relatively easy under the assumption that they are viewed from the front and are at a significant distance. However, these effects must be considered in an experiment where signals are received from various directions while changing positions. We derived the corresponding change in the modulated optical signal pattern and the overall effect on BMH demodulation as follows.

The optical signal pattern corresponding to b' and a', i.e., the ratio of 1:4, varies depending on the direction in which they are viewed. In our method, as signal restoration proceeds based on an additional slot information that emits b' in all the channels, we consider that the value a' varies while b' is fixed. If the revised matrix is $\boldsymbol{H'_{\mathrm{BMH}}}$ and the change of a' in the i-th channel is δ_i, the received signal $\boldsymbol{r'}$ is derived as follows:

$$\begin{aligned}\boldsymbol{r'} &= \boldsymbol{s} \times \boldsymbol{H'_{\mathrm{BMH}}} \\ &= \boldsymbol{s} \times \begin{bmatrix} a'+\delta_1 & b' & \cdots & b' \\ b' & a'+\delta_2 & \cdots & b' \\ \vdots & \vdots & \ddots & \vdots \\ b' & b' & \cdots & a'+\delta_n \end{bmatrix} \\ &= \boldsymbol{s} \times (\boldsymbol{H_{\mathrm{BMH}}} + \boldsymbol{\Delta}), \quad \boldsymbol{\Delta} = diag(\delta_1, \delta_2, \cdots, \delta_n). \end{aligned} \tag{22}$$

Using (13)-(14), $\boldsymbol{r'^*}$ and $\boldsymbol{s'^*}$ are calculated as:

$$\boldsymbol{r'^*} = \boldsymbol{r'} + b_m \cdot sum(\boldsymbol{s}) = \boldsymbol{s} \times \boldsymbol{H_{\mathrm{MH}}} + \boldsymbol{s} \times \boldsymbol{\Delta} \tag{23}$$

$$\boldsymbol{s'^*} = \boldsymbol{r'^*} \times \boldsymbol{H_{\mathrm{MH}}^{\top}} = \boldsymbol{s} \times m^2\boldsymbol{I} + \boldsymbol{s} \times \boldsymbol{\Delta} \times \boldsymbol{H_{\mathrm{MH}}^{\top}} \tag{24}$$

and the i-th signal is derived as follows:

$$\begin{aligned} s'^*(i) &= m^2 s_i + a \cdot s_i\delta_i + b \cdot \textstyle\sum_{k(\neq i)}^{n} s_k\delta_k \\ &= (m^2 - (b-a)\delta_i)s_i + b \cdot \textstyle\sum_{k}^{n} s_k\delta_k \\ &= (m^2 - m\delta_i)s_i + b \cdot \textstyle\sum_{k}^{n} s_k\delta_k. \end{aligned} \tag{25}$$

In this equation, the second term is applied to all the signals. Besides, in the first term, the magnitude of the signal varies with δ_i, i.e., as the δ value increases, the relative RSS value becomes smaller. From (8), when the RSS is low, the distance between the LED and the PD is farther. However, the δ value is affected by the direction in which the LED array is viewed. If the signal is received from a direction close to a single driving LED, the signals of the remaining three LEDs are relatively weak, and a signal with ratio 4:1 is received, for example, changed as a 3.5:1 ratio. This indicates that the absolute value of the negative number a' has been reduced by 0.5 and δ has a value of +0.5. Likewise, if the signal is received from a direction far from the single driving LED, the three-LED signal is perceived to be stronger such that δ has a negative value. In summary,

$$\begin{cases} \text{closer to single LED} \rightarrow \delta \uparrow \rightarrow \text{RSS} \downarrow \\ \qquad\qquad\qquad \rightarrow d \uparrow \rightarrow \text{further from LED array} \\ \text{further from single LED} \rightarrow \delta \downarrow \rightarrow \text{RSS} \uparrow \\ \qquad\qquad\qquad \rightarrow d \downarrow \rightarrow \text{closer to LED array} \end{cases} \tag{26}$$

Through this relationship, an in-depth analysis of the positioning error direction is conducted. The positioning uses the information of the strongest signal, that is, the signal of the three closest LEDs; hence, all the test cases are classified according to the LEDs as follows:

- Area 1. LED 1, 2, 3 used: 1, 2, 3, 8, 9, 14, 19, 23
- Area 2. LED 2, 3, 4 used: 4, 10, 11, 15, 16, 17, 20, 21, 24, 25, 26
- Area 3. LED 3, 4, 5 used: 5, 6, 7, 12, 13, 18, 22, 27

As shown in Fig. 12, LED 1 is close to a single driving element for all test cases in area 1, and LEDs 2 and 3 are closer to the simultaneous driving bundle. Therefore, the determined position of the receiver appears to be far from LED 1 but close to LEDs 2 and 3; in fact, it is observed that most cases follow this configuration. In area 2, the position of the receiver is measured uniformly while looking at the side of all the three

LED arrays. As the position of the receiver becomes closer to LED 4, it becomes more affected by the single driving unit of LEDs 2 and 3. In area 3, the position is mainly affected by the single driving unit of LEDs 3 and 4, and it is observed that the red circle is concentrated close to LED 5.

Through an in-depth analysis in this subsection, it was confirmed that most of the results were affected by the LED placement. Meanwhile, some nodes (10, 15, 20, 24), which were judged to have a relatively insignificant impact, showed much better performance than other nodes. This indicates that although the results of this experiment are excellent, if the structure of the transmitter is supplemented with a completely symmetrical LED arrangement or a single LED that is capable of controlling the intensity is used, better results can be obtained.

VI. CONCLUSION

In this paper, a new multiple access technique suitable for IM/DD-based VLP systems was presented. The proposed method utilizes a conventional M-H matrix with guaranteed orthogonality and no order constraints, and optimizes power consumption by adding and subtracting bias before and after signal transmission. Moreover, several considerations and some constraints for evaluating the modulation schemes were presented. Based on these conditions, the superiority of the proposed method was verified by comparing it with the conventional bandpass and baseband methods. Additionally, a 5-order BMH method was implemented through low-cost and low-complexity hardware, and the performance was quantitatively evaluated by a positioning experiment. The positioning result showed an average error of 3.18 cm, and the result within 80 % showed an error of less than 5 cm. Through further in-depth analysis, we showed that better results could be obtained depending on an additional correction or symmetrical hardware configuration. The proposed technique is optimized for power consumption, has no restrictions on the number of channels or driving frequency, and is relatively simple to implement. Therefore, the proposed method is suitable for both wide and complex VLP systems, as well as narrow and ordered spaces.

REFERENCES

[1] M. Yasir, S.-W. Ho, and B. N. Vellambi, "Indoor position tracking using multiple optical receivers," *J. Lightw. Technol.*, vol. 34, no. 4, pp. 1166–1176, Feb. 15, 2016.

[2] Q. Wang and H. Luo, "Light positioning: A high-accuracy visible light indoor positioning system based on attitude identication and propagation model," *Int. J. Distrib. Sensor Netw.*, vol. 14, no. 2, p. 114, Feb. 2018.

[3] Y. Cai, W. Guan, Y. Wu, C. Xie, Y. Chen, and L. Fang, "Indoor high precision three-dimensional positioning system based on visible light communication using particle swarm optimization," *IEEE Photon. J.*, vol. 9, no. 6, Dec. 2017, Art. no. Art. no. 7908120.

[4] D. Karunatilaka, F. Zafar, V. Kalavally, and R. Parthiban, "LED based indoor visible light communications: State of the art," *IEEE Commun. Surveys Tuts.*, vol. 17, no. 3, pp. 1649–1678, 3rd Quart., 2015.

[5] D. Kim, J. K. Park, and J. T. Kim, "Three-dimensional VLC positioning system model and method considering receiver tilt," *IEEE Access*, vol. 7, pp. 132205–132216, 2019.

[6] A. Sevincer, A. Bhattarai, M. Bilgi, M. Yuksel, and N. Pala, "LIGHTNETs: Smart lighting and mobile optical wireless networks—A survey," *IEEE Commun. Surveys Tuts.*, vol. 15, no. 4, pp. 1620–1641, 4th Quart., 2013.

[7] H.-S. Kim, D.-R. Kim, S.-H. Yang, Y.-H. Son, and S.-K. Han, "An indoor visible light communication positioning system using a RF carrier allocation technique," *J. Lightw. Technol.*, vol. 31, no. 1, pp. 134–144, Jan. 2013.

[8] S.-H. Yang, H.-S. Kim, Y.-H. Son, and S.-K. Han, "Three-dimensional visible light indoor localization using AOA and RSS with multiple optical receivers," *J. Lightw. Technol.*, vol. 32, no. 14, pp. 2480–2485, Jul. 1, 2014.

[9] M. Yasir, S.-W. Ho, and B. N. Vellambi, "Indoor positioning system using visible light and accelerometer," *J. Lightw. Technol.*, vol. 32, no. 19, pp. 3306–3316, Oct. 1, 2014.

[10] S. Yamaguchi, V. V. Mai, T. C. Thang, and A. T. Pham, "Design and performance evaluation of VLC indoor positioning system using optical orthogonal codes," in *Proc. IEEE 5th Int. Conf. Commun. Electron. (ICCE)*, Jul. 2014, pp. 54–59.

[11] Y.-A. Chen, Y.-T. Chang, Y.-C. Tseng, and W.-T. Chen, "A framework for simultaneous message broadcasting using CDMA-based visible light communications," *IEEE Sensors J.*, vol. 15, no. 12, pp. 6819–6827, Dec. 2015.

[12] J. K. Park, T.-G. Woo, M. Kim, and J. T. Kim, "Hadamard matrix design for a low-cost indoor positioning system in visible light communication," *IEEE Photon. J.*, vol. 9, no. 2, pp. 1–10, Apr. 2017.

[13] S. De Lausnay, L. De Strycker, J.-P. Goemaere, B. Nauwelaers, and N. Stevens, "Design of a visible light communication transmitter for the evaluation of a wide range of modulation techniques," in *Proc. 2nd Int. Workshop Opt. Wireless Commun. (IWOW)*, Oct. 2013, pp. 30–34.

[14] J. M. Kahn and J. R. Barry, "Wireless infrared communications," *Proc. IEEE*, vol. 85, no. 2, pp. 265–298, Feb. 1997.

[15] J. Armstrong and A. J. Lowery, "Power efficient optical OFDM," *Electron. Lett.*, vol. 42, no. 6, pp. 370–372, Mar. 2006.

[16] S. D. Dissanayake and J. Armstrong, "Comparison of ACO-OFDM, DCO-OFDM and ADO-OFDM in IM/DD systems," *J. Lightw. Technol.*, vol. 31, no. 7, pp. 1063–1072, Apr. 2013.

[17] I. Alonso-González, D. Sánchez-Rodríguez, C. Ley-Bosch, and M. Quintana-Suárez, "Discrete indoor three-dimensional localization system based on neural networks using visible light communication," *Sensors*, vol. 18, no. 4, p. 1040, Mar. 2018.

[18] J. He, C.-W. Hsu, Q. Zhou, M. Tang, S. Fu, D. Liu, L. Deng, and G.-K. Chang, "Demonstration of high precision 3D indoor positioning system based on two-layer ANN machine learning technique," in *Proc. Opt. Fiber Commun. Conf. (OFC)*, 2019, p. 2.

[19] P. Du, S. Zhang, C. Chen, H. Yang, W.-D. Zhong, R. Zhang, A. Alphones, and Y. Yang, "Experimental demonstration of 3D visible light positioning using received signal strength with low-complexity trilateration assisted by deep learning technique," *IEEE Access*, vol. 7, pp. 93986–93997, 2019.

[20] H. Zhang, J. Cui, L. Feng, A. Yang, H. Lv, B. Lin, and H. Huang, "High-precision indoor visible light positioning using deep neural network based on the Bayesian regularization with sparse training point," *IEEE Photon. J.*, vol. 11, no. 3, Jun. 2019, Art. no. 7903310.

[21] D. H. Mai, H. D. Le, T. V. Pham, and A. T. Pham, "Design and performance evaluation of large-scale VLC-based indoor positioning systems under impact of receiver orientation," *IEEE Access*, vol. 8, pp. 61891–61904, 2020.

[22] Q. K. Trinh, P. Fan, and E. M. Gabidulin, "Multi-level Hadamard matrices and zero correlation zone sequences," *Electron. Lett.*, vol. 42, pp. 748–750, Jun. 2006.

[23] J. Park, C.-J. Lee, and J. Kim, "Analysis of multi-level simultaneous driving technique for capacitive touch sensors," *Sensors*, vol. 17, no. 9, p. 2016, Sep. 2017.

[24] J. K. Park and J. T. Kim, "Delay-tolerant multiplexed stimulation and its processing method for multi-channel active sensors," *IEEE Access*, vol. 6, pp. 46762–46770, 2018.

[25] Y. Yang, C. Chen, P. Du, X. Deng, J. Luo, W.-D. Zhong, and L. Chen, "Low complexity OFDM VLC system enabled by spatial summing modulation," *OSA Opt. Exp.*, vol. 27, no. 21, pp. 30788–30795, Oct. 2019.

[26] C. Hu, C. Chen, M. Guo, Y. Yang, J. Luo, and L. Chen, "Optical-spatial-summing-based NOMA with fine-grained power allocation for VLC-enabled IoT applications," *OSA Opt. Lett.*, vol. 45, no. 17, pp. 4927–4930, Sep. 2020.

[27] *Luxeon Star LEDs*. Accessed: Dec. 5, 2020. [Online]. Available: https://support.luxeonstar.com/hc/en-us

[28] *IEEE Standard for Information Technology—Local and Metropolitan Area Networks—Specific Requirements—Part 15.4: Wireless Medium Access Control (MAC) and Physical Layer (PHY) Specifications for Low Rate Wireless Personal Area Networks (WPANs)*, Standard 802.15.4-2006, Sep. 2006.
[29] S. M. Berman, D. S. Greenhouse, I. L. Bailey, R. D. Clear, and T. W. Raasch, "Human electroretinogram responses to video displays, fluorescent lighting and other high frequency sources," *Optometry Vis. Sci.*, vol. 68, pp. 645–662, Aug. 1991.
[30] A. J. C. Moreira, R. T. Valadas, and A. M. de Oliveira Duarte, "Optical interference produced by artificial light," *Wireless Netw.*, vol. 3, no. 2, pp. 131–140, 1997.
[31] D. Wood, *Optoelectronic Semiconductor Devices*. Upper Saddle River, NJ, USA: Prentice-Hall, 1994.
[32] A. E. Iverson and D. L. Smith, "Mathematical modeling of photoconductor transient response," *IEEE Trans. Electron Devices*, vol. 34, no. 10, pp. 2098–2107, Oct. 1987.
[33] N. Dinur and D. Wulich, "Peak-to-average power ratio in high-order OFDM," *IEEE Trans. Commun.*, vol. 49, no. 6, pp. 1063–1072, Jun. 2001.
[34] D. Crnkoviá, "A series of regular Hadamard matrices," *Des., Codes Cryptogr.*, vol. 39, no. 2, pp. 247–251, May 2006.

DUCKYONG KIM received the B.S. degree from the Department of Electrical and Computer Engineering, Sungkyunkwan University, Suwon, South Korea, in 2017, where he is currently pursuing the integrated M.S. and Ph.D. degrees. His current research interests include the sensor signal processing, recognition, and location-aware embedded system design.

JONG KANG PARK (Member, IEEE) received the B.S. and M.S. degrees in electric, electronics, and computer engineering and the Ph.D. degree in electric and electronics engineering from Sungkyunkwan University, South Korea, in 2001, 2003, and 2008, respectively. From 2008 to 2013, he was with Samsung Electronics, where he designed commercial touch sensor ICs and multi-touch algorithms. He is currently a Research Professor with the School of Electronic and Electrical Engineering, Sungkyunkwan University. His research interests include concurrent signal multiplexing and processing techniques, and fault-tolerant embedded system designs.

JONG TAE KIM (Member, IEEE) received the B.S. degree in electronics engineering from Sungkyunkwan University, South Korea, in 1982, and the M.S. and Ph.D. degrees in electrical and computer engineering from the University of California at Irvine, Irvine, CA, USA, in 1987 and 1992, respectively. From 1991 to 1993, he was with the Aerospace Corporation, Elsegundo, CA, USA. He was a full-time Lecturer with Chunbuk National University, South Korea, from 1993 to 1995. He is currently a Professor with the School of Electronic and Electrical Engineering, Sungkyunkwan University, where he has been since 1995. His research interests include sensor systems, brain-inspired computing and architecture, embedded systems, and the IoT.